A Linear Array of Skewed Dipoles With Asymmetric Radiation Pattern for Angular Filtering

Yepes, C.; Gandini, E.; Monni, S.; Neto, A.; Vliet, F. E. van; Cavallo, D.

DOI
10.1109/LAWP.2020.2971347

Publication date
2020

Document Version
Final published version

Published in
IEEE Antennas and Wireless Propagation Letters

A Linear Array of Skewed Dipoles With Asymmetric Radiation Pattern for Angular Filtering

Cristina Yepes, *Student Member, IEEE*, Erio Gandini, *Member, IEEE*, Stefania Monni, *Senior Member, IEEE*, Andrea Neto, *Fellow, IEEE*, Frank E. van Vliet, *Senior Member, IEEE*, and Daniele Cavallo, *Senior Member, IEEE*

***Abstract*—In this letter, we present a design of a linear array of tilted dipoles to achieve radiation patterns with asymmetric angular filtering characteristics. To realize the asymmetric radiation, the dipole elements are spaced by a distance larger than half a wavelength, thus allowing for grating lobes to occur in the visible region. Moreover, the dipoles are loaded with artificial dielectrics to increase the front-to-back ratio and consequently to enable higher gain in certain desired angular regions. Based on the design, a linear array with ten elements is manufactured and tested. The measured results show the ability of such an array to achieve stable gain from broadside up to 90° scanning while implementing a stopband angular filter for negative scanning angles.**

***Index Terms*—Angular filtering, antenna arrays, pattern asymmetry, tilted dipole array.**

I. Introduction

MODERN antenna arrays for radar and communication applications often operate in environments where a multitude of sensors and radiating systems need to coexist. To avoid interference between different antenna systems, the implementation of angular filtering functions can be beneficial. Moreover, in some of the mentioned applications, it is sometimes not required for the antennas to exhibit a field-of-view that is symmetric with respect to broadside, but rather a gain profile that is stable over a certain desired angular region. For instance, to improve the system capacity of base-stations antennas, a down-tilt of the radiation toward the ground was employed to increase the signal reception from the mobile device [1], [2]. In satellite communications, tilting the embedded pattern of the individual elements of an antenna array was implemented to achieve a gain enhancement for large scan angles within a limited azimuth region [3], [4]. The entire field-of-view was then covered by mechanical rotation of the array along its axis.

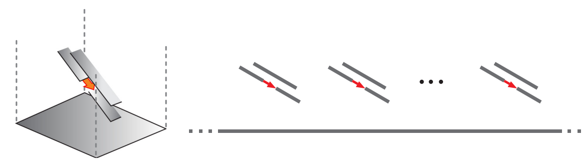
(a) (b)

Fig. 1. Array of titled stacked dipole elements in the presence of an infinite ground plane. (a) 3-D view of the unit cell. (b) Side view.

Pattern shaping can be achieved with aperture antennas in combination with partially reflective surfaces [5]–[7]. Angular filters have been realized mainly with frequency selective surfaces or leaky-wave structures [8]–[13], with the aim of increasing the directivity of the array element to reduce the levels of the sidelobes or grating lobes. In [14] and [15], rectilinear leaky-wave antennas were synthesized to realize radiation patterns with angular selectivity and asymmetry properties. However, with this concept, the entire array radiates a broad beam with an angular passband filtering function, precluding the possibility to generate highly directive beams that can be scanned within the field-of-view of interest.

In this letter, the proposed approach is to realize an antenna array where the single element exhibits a radiation pattern with angular selectivity, asymmetric with respect to broadside. The resulting active element pattern will filter the array factor of the entire array while scanning, providing high gain only in the desired field of view. Recently in [16], we showed that one effective way to achieve asymmetric active element patterns is by enhancing the directivity of the element (e.g., with a dipole loaded by a parasitic strip as director) and by rotating the array element around their center, as shown in Fig. 1. In [16], the fundamental radiation properties of arrays of stacked dipoles were investigated with a spectral method of moments. The results are consistent with the general theory of arrays with asymmetric elements given in [17] and [18]. Based on the findings provided in [16], we propose here the design of a linear array of tilted dipole elements to achieve asymmetric radiation characteristics. The dipoles are loaded with artificial dielectrics

Manuscript received January 7, 2020; revised January 24, 2020; accepted January 28, 2020. Date of publication February 6, 2020; date of current version March 3, 2020. This work was supported by the TNO Ph.D. funding. *(Corresponding author: Cristina Yepes.)*

Cristina Yepes is with the Microelectronics Department, Faculty of Electrical Engineering, Mathematics and Computer Science, Delft University of Technology, Delft 2628 CD, The Netherlands, and also with the Department of Radar Technology, TNO, The Hague 2597 AK, The Netherlands (e-mail: c.yepesjulia@tudelft.nl).

Erio Gandini and Stefania Monni are with the Department of Radar Technology, TNO, The Hague 2597 AK, The Netherlands (e-mail: erio.gandini@tno.nl; stefania.monni@tno.nl).

Andrea Neto and Daniele Cavallo are with the Microelectronics Department, Faculty of Electrical Engineering, Mathematics and Computer Science, Delft University of Technology, Delft 2628 CD, The Netherlands (e-mail: A.Neto@tudelft.nl; d.cavallo@tudelft.nl).

Frank E. van Vliet is with the Department of Radar Technology, TNO, The Hague 2597 AK, The Netherlands, and also with the Center for Array Technology, University of Twente, Enschede 7522 NB, The Netherlands (e-mail: frank.vanvliet@tno.nl).

Digital Object Identifier 10.1109/LAWP.2020.2971347

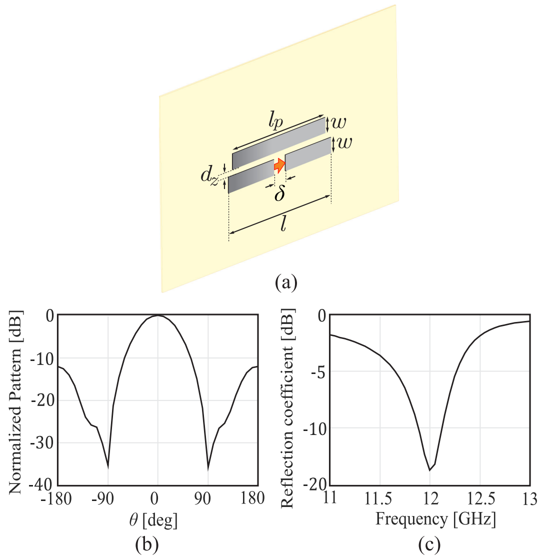

Fig. 2. (a) Single element of a stacked dipole printed on a PCB, (b) E-plane pattern, and (c) reflection coefficient of the single element described in (a).

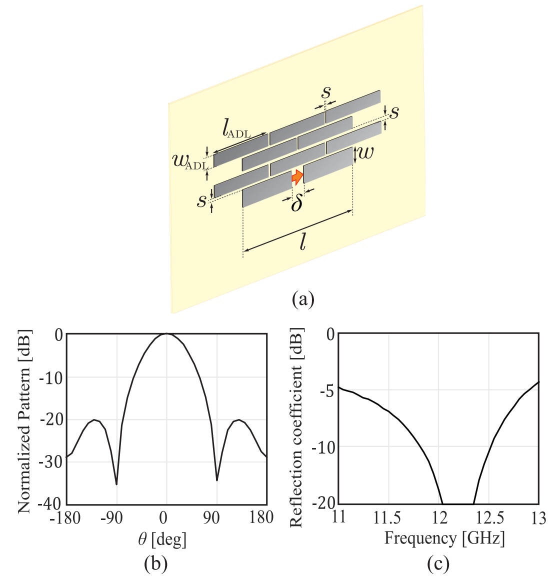

Fig. 3. (a) Single element of a dipole loaded with AD layer printed on a PCB, and its (b) single element E-plane pattern, and (c) reflection coefficient.

(ADs) to increase the gain in certain desired angular regions. An implementation of the array based on printed circuit technology (PCB) is proposed and a prototype linear array with ten elements is manufactured and tested.

II. Unit Cell Design

In [16], the guidelines to design an array with asymmetric radiation properties were discussed. The main unit cell under analysis consisted in an idealized element with infinitely thin flat strip dipoles, fed with a delta-gap excitation, as shown in Fig. 1(a). In this section, we propose a realistic implementation of the element, based on PCB technology.

A. Single Dipole Element With Parasitic Loading

To enable a simple realization of the flat strip dipole element, we first consider an equivalent isolated element where the active dipole and the parasitic strip are printed on a vertically oriented thin dielectric slab. Fig. 2(a) shows the considered structure with the characteristic geometrical parameters. The dimensions of the elements are chosen as: $l = 0.41\lambda_0$, $l_p = 0.37\lambda_0$, $w = 0.05\lambda_0$, $\delta = 0.01\lambda_0$, and $d_z = 0.7\lambda_0$, where λ_0 is the wavelength at 12 GHz. The dielectric slab selected for the design is Rogers RO4530 TM with relative dielectric constant $\varepsilon_r = 3.66$ and thickness $t = 101$ μm. The dimensions are optimized so that the directivity of the element is maximized. The simulated E-plane pattern of the single element in free space is reported in Fig. 2(b), at 12 GHz, exhibiting a front-to-back ratio of 12 dB. Fig. 2(c) depicts the simulated reflection coefficient of the element, showing a rather narrow bandwidth of only 2% centered at 12 GHz, normalized to a low impedance of 10 Ω.

To enhance the front-to-back ratio of the element as well as the bandwidth, a solution consisting of a tilted dipole element loaded with three layers of AD is proposed in Fig. 3(a). The AD consists of subwavelength metal strips on the same plane of

TABLE I
Geometrical Parameter of Element in Fig. 3, With Respect to the Wavelength λ_0 at 12 GHz

l	w	δ	l_{ADL}	w_{ADL}	s
$0.434\lambda_0$	$0.05\lambda_0$	$0.05\lambda_0$	$0.212\lambda_0$	$0.0336\lambda_0$	$0.01\lambda_0$

the dipole. This element is also printed on a vertical PCB with a dielectric with the same relative permittivity and thickness as for the stacked dipole solution ($\varepsilon_r = 3.66$, $t = 101$ μm). The dimensions, reported in Table I, were tuned to enhance the directivity of the element. The single-element E-plane pattern at 12 GHz and the reflection coefficient are shown in Fig. 3(b) and (c), respectively. The dipole loaded with AD has a back lobe with -20 dB level and a bandwidth of 6%, with respect to the normalization impedance of 30 Ω. The simulated gain is 6.8 dB, whereas it is 2.4 dB for an isolated dipole without AD.

B. Infinite Array of Dipoles Loaded With ADs

We now consider the element in Fig. 3(a), tilted by an angle α and embedded in an infinite linear array environment, in the presence of a backing reflector. The resulting unit cell is depicted in Fig. 4(a). The distance between the center of the dipole and the infinite ground plane is $h_{\mathrm{gp}} = 0.25\lambda_0$, and the total height of the dielectric is $h = 0.7\lambda_0$.

To describe the angular filtering function, let us imagine to divide the angular region between -90° and 90° in two portions, one desired, where high gain is wished for, and one undesired, where gain suppression is targeted [see Fig. 4(b)]. If the angle bounding these two regions is referred to as θ_{drop}, from the study done in [16], we can derive an optimal interelement spacing and inclination angle of the elements to achieve a desired θ_{drop}. For example, the choice of $\theta_{\mathrm{drop}} = -20^\circ$ results in an optimal period of $d_x = 0.75\lambda_0$ and an optimal inclination angle of $\alpha = 40^\circ$.

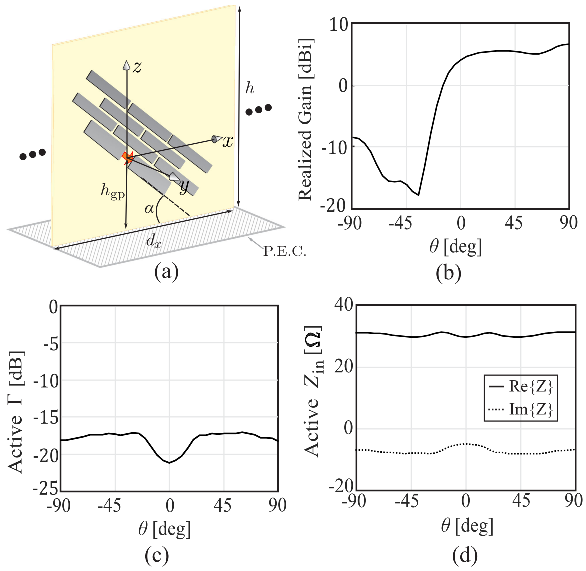

Fig. 4. (a) Infinite 1-D array unit cell of a tilted dipole with AD loading in the presence of a backing reflector. (b) E-plane realized gain active element pattern, (c) active reflection coefficient, and (d) active input impedance, versus scan angle.

Fig. 4(b) reports the simulated active element pattern in the E-plane at 12 GHz. The radiation pattern shows a clear drop in gain in the range $-90^\circ < \theta < -30^\circ$, a roll-off region centered around the target value $\theta_{\text{drop}} = -20^\circ$, and almost constant value for angles between 0° and 90°. The active reflection coefficient at 12 GHz and the active input impedance are shown in Fig. 4(c) and (d), respectively, as a function of the scan angle. It can be noted that the impedance is almost constant with scan angle, which is a consequence of the low mutual coupling between the elements. Indeed, the large interelement spacing ($0.75\lambda_0$) yields low coupling; thus, the active input impedance is close to the passive input impedance and hardly dependent on the scan angle.

C. Feed Design

The last step of the unit cell design consists in replacing the ideal delta-gap feed with a realistic feeding structure. We employ a microstrip feeding line with a Marchand balun to avoid the excitation of common mode currents. A two-quarter-wave section transmission line is used to transform the $30\,\Omega$ impedance at the antenna terminals up to $50\,\Omega$ at the coaxial connector input. For the sake of simple realization, the horizontal ground plane is replaced by a vertical ground plane printed on the same PCB as the dipole and the feeding lines [see Fig. 5(a)]. The parameters of the feed structure are illustrated in Fig. 5(b) and (c) and their values are in Table II.

Fig. 6(a) shows the simulated active element pattern, comparing directivity and realized gain. The simulation includes the feeding lines and the connector and accounts for the material losses, both metal and dielectric. The difference between directivity and gain is about 0.8 dB, which corresponds to a simulated efficiency of 83%. We can observe that gain levels in the undesired region are about -15 dB below the maximum

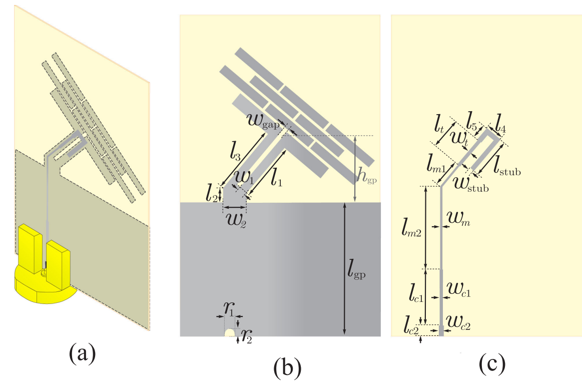

Fig. 5. (a) 3-D view of the array element with an SMA connector, (b) front and (c) back of the unit cell design with the radiating element, the feeding lines with a Marchand balun and a vertical ground plane.

TABLE II
GEOMETRICAL PARAMETER OF THE FEED STRUCTURE (IN mm)

w_{gap}	l_1	l_2	l_3	l_{gp}	w_1	w_2	l_{stub}
0.4	6.55	1.39	5.5	12.5	0.8	2.21	3.85

l_t	l_{m1}	l_{m2}	l_4	l_5	l_{c1}	l_{c2}	w_{stub}
3	2.6	14.04	1.65	1.35	5.25	1	0.45

w_t	w_m	w_{c1}	w_{c2}	r_1	r_2
0.3	0.18	0.3	0.6	1.02	0.75

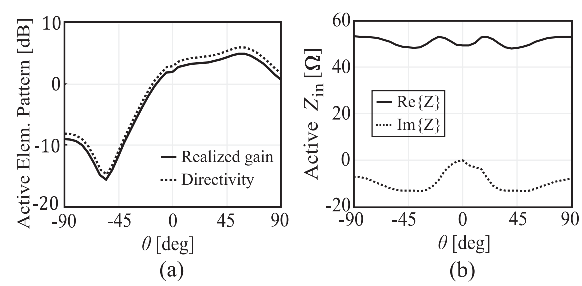

Fig. 6. (a) E-plane radiation pattern and (b) input impedance while varying the scanning angle of the unit cell shown in Fig. 5(a).

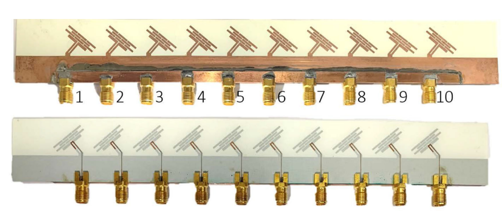

Fig. 7. Photograph of the front and back of prototype array.

gain, similarly to the previous results for the ideal feed. Fig. 6(b) shows the active input impedance at 12 GHz versus the scan angle. The impedance is well matched to 50 Ω and marginally varying with the scan angle.

III. ARRAY PROTOTYPE

Based on the unit cell design presented in Section II, a finite linear array comprising ten elements was manufactured (see Fig. 7). A subset of the array S-parameters was measured, i.e.,

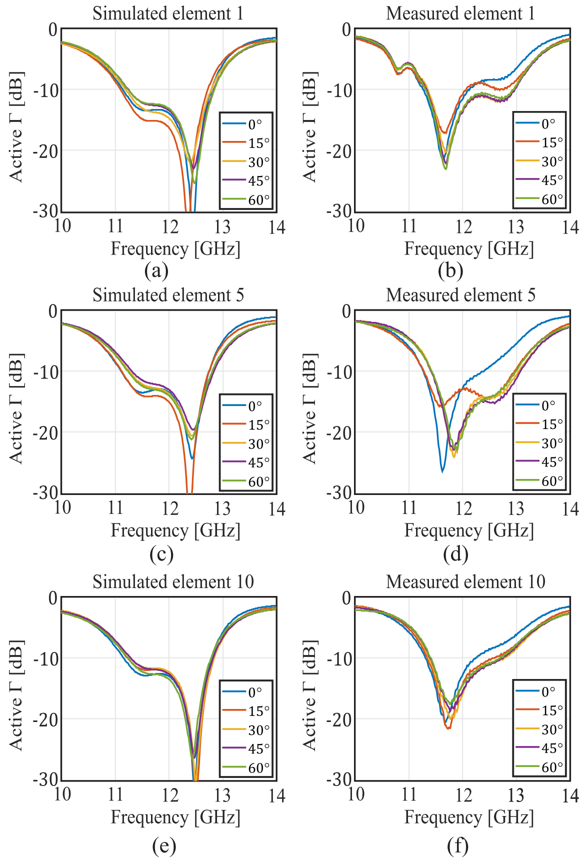

Fig. 8. Simulated and measured active reflection coefficient for (a) and (b) element 1, (c) and (d) element 5, and (e) and (f) element 10.

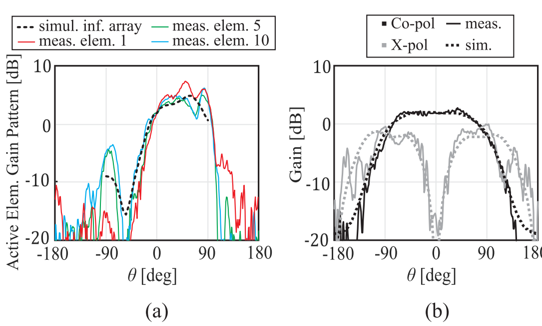

Fig. 9. (a) Active element pattern (gain) of three elements of the array, compared with infinite array simulations. (b) Copolar and cross-polar H-plane gain pattern of element 5 of the array, compared with simulations.

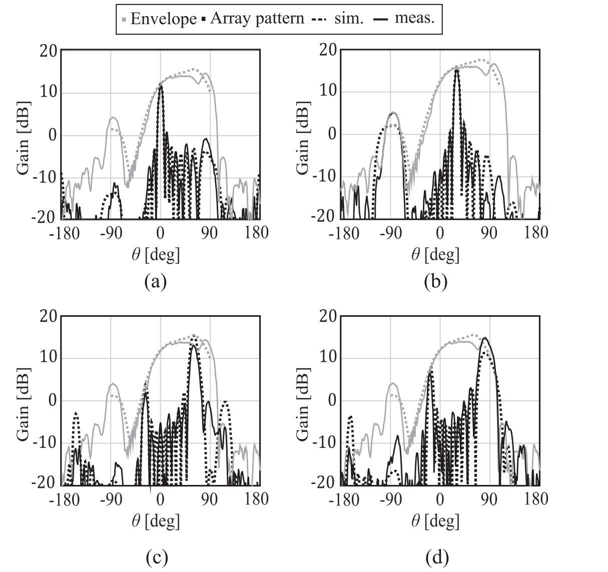

Fig. 10. Measured and simulated array gain patterns for different scan angles: scan to (a) $\theta = 0°$, (b) $\theta = 20°$, (c) $\theta = 60°$, and (d) $\theta = 90°$.

the coupling coefficients of the elements with indexes 1, 5, and 10 with all the others. This allows us to compute the active reflection coefficient of one central element (element 5) and the two edge elements (elements 1 and 10) for different scan angles. The results are shown in Fig. 8. Simulations of the finite array are also reported in the same figure for comparison. The elements show a matching bandwidth of about 10%, which is almost constant when scanning.

The measured gain active element patterns in the E-plane are reported in Fig. 9(a), for a few array elements, at a frequency of 12 GHz. Because of truncation effects in the finite array, the gain patterns differ for each element. For example, element 1 displays a lower level sidelobe pointing at $-90°$, compared to other elements. All measured radiation patterns closely resemble the active element pattern simulated with the infinite array approximation, also shown in Fig. 9(a). Larger discrepancies occur at angles close to $\pm 90°$. This is due to some reflections from the plastic frame holding the antenna, used for the measurements.

The H-plane gain pattern of the central element of the array is shown in Fig. 9(b), comparing simulation with measurements. Also the cross-polarized component is shown in the figure. In fact, in the E-plane, the cross-polar is not affected by the tilt of the dipoles nor by the feeding structure since both the planar and vertical components of the current radiate copolar fields. However, in the H-plane, the cross-polar component increases for angles away from broadside due to the tilting and the radiating currents.

By summing the measured active element patterns with the proper phases, we can also estimate the total array patterns. The resulting gain patterns are shown in Fig. 10, compared with simulations. When scanning to 20°, the grating lobe entering in the visible region can be observed at $-90°$, but its level remains -10 dB below the maximum, because it is weighted by the filtering function of the element pattern.

IV. Conclusion

We presented the design of a linear array of dipoles with asymmetric radiation properties. The array elements consist of tilted dipoles with parasitic AD layers to enhance their gain. The pattern of such an element can be designed to exhibit a high-gain desired region for angles in the range $\theta_{\text{drop}} < \theta < 90°$ and a low-gain undesired region for $-90° < \theta < \theta_{\text{drop}}$. The angle θ_{drop} can be controlled by the interelement distance, whereas the difference in gain between the desired and undesired regions can be optimized by the tilt angle of the elements. A prototype array based on this concept was presented, showing a good comparison between simulated and measured characteristics.

REFERENCES

[1] D. Sugimura, M. Arai, K. Sakaguchi, K. Araki, and T. Sotoyama, "A study on beam tilt angle of base station antennas for base station cooperation systems," in *Proc. IEEE 22nd Int. Symp. Pers., Indoor Mobile Radio Commun.*, Toronto, ON, Canada, 2011, pp. 2374–2378.

[2] I. Kim and Y. Rahmat-Samii, "Electromagnetic band gap-dipole sub-array antennas creating an enhanced tilted beams for future base station," *Microw., Antennas Propag.*, vol. 9, no. 4, pp. 319–327, Mar. 2015.

[3] F. Tiezzi, D. Llorens, C. Dominguez, and M. Fajardo, "A compact Ku-band transmit/receive low-profile antenna for broadband mobile satellite communications," in *Proc. 4th Eur. Conf. Antennas Propag.*, Barcelona, Spain, 2010, pp. 1–4.

[4] J. Biosca, D. Llorens, and M. C. Viganó, "Side-lobe reduction with overlapped beam-forming network for Ku-band hybrid antenna array," in *Proc. 10th Eur. Conf. Antennas Propag.*, Davos, Switzerland, 2016, pp. 1–5.

[5] G. Von Trentini, "Partially reflecting sheet arrays," *IRE Trans. Antennas Propag.*, vol. AP-4, no. 4, pp. 666–671, Oct. 1956.

[6] J. R. James, S. J. A. Kinany, P. D. Peel, and G. Andrasic, "Leaky-wave multiple dichroic beamformers," *Electron. Lett.*, vol. 25, no. 18, pp. 1209–1211, Aug. 1989.

[7] A. P. Feresidis and J. C. Vardaxoglou, "High gain planar antenna using optimised partially reflective surfaces," *IEE Proc.—Microw., Antennas Propag.*, vol. 148, no. 6, pp. 345–350, Dec. 2001.

[8] P. Franchi and R. Mailloux, "Theoretical and experimental study of metal grid angular filters for sidelobe suppression," *IEEE Trans. Antennas Propag.*, vol. AP-31, no. 3, pp. 445–450, May 1983.

[9] D. R. Jackson and A. A. Oliner, "A leaky-wave analysis of the high-gain printed antenna configuration,"*IEEE Trans. Antennas Propag.*, vol. AP-36, no. 7, pp. 905–910, Jul. 1988.

[10] Y. J. Lee, S. H. Jeong, W. S. Park, J. S. Yun, and S. I. Jeon, "Multilayer spatial angular filter with airgap tuners to suppress grating lobes of 4×1 array antenna," *Electron. Lett.*, vol. 39, no. 1, pp. 15–17, Jan. 2003.

[11] R. Gardelli, M. Albani, and F. Capolino, "Array thinning by using antennas in a Fabry–Perot cavity for gain enhancement,"*IEEE Trans. Antennas Propag.*, vol. 54, no. 7, pp. 1979–1990, Jul. 2006.

[12] D. Blanco, N. Llombart, and E. Rajo-Iglesias, "On the use of leaky wave phased arrays for the reduction of the grating lobe level," *IEEE Trans. Antennas Propag.*, vol. 62, no. 4, pp. 1789–1795, Apr. 2014.

[13] D. Blanco, E. Rajo-Iglesias, S. Maci, and N. Llombart, "Directivity enhancement and spurious radiation suppression in leaky-wave antennas using inductive grid metasurfaces," *IEEE Trans. Antennas Propag.*, vol. 63, no. 3, pp. 891–900, Mar. 2015.

[14] P. Burghignoli, F. Frezza, A. Galli, and G. Schettini, "Synthesis of broad-beam patterns through leaky-wave antennas with rectilinear geometry," *IEEE Antennas Wireless Propag. Lett.*, vol. 2, pp. 136–139, 2003.

[15] A. J. Martinez-Ros, J. L. Gómez-Tornero, and G. Goussetis, "Multifunctional angular bandpass filter SIW leaky-wave antenna," *IEEE Antennas Wireless Propag. Lett.*, vol. 16, pp. 936–939, 2017.

[16] C. Yepes, E. Gandini, S. Monni, A. Neto, F. E. van Vliet, and D. Cavallo, "Analysis of tilted dipole arrays: Impedance and radiation properties," *IEEE Trans. Antennas Propag.*, vol. 68, no. 1, pp. 254–265, Jan. 2020.

[17] A. K. Bhattacharyya, "Active element pattern symmetry for asymmetrical element arrays," *IEEE Antennas Wireless Propag. Lett.*, vol. 6, pp. 275–278, 2007.

[18] H. Steyskal, "On the merit of asymmetric phased array elements," *IEEE Trans. Antennas Propag.*, vol. 61, no. 7, pp. 3519–3524, Jul. 2013.